Assembly of the cochlear gap junction macromolecular complex requires connexin 26

Kazusaku Kamiya,[1] Sabrina W. Yum,[2,3] Nagomi Kurebayashi,[4] Miho Muraki,[1] Kana Ogawa,[1] Keiko Karasawa,[1] Asuka Miwa,[1] Xueshui Guo,[2] Satoru Gotoh,[5] Yoshinobu Sugitani,[5] Hitomi Yamanaka,[5] Shioko Ito-Kawashima,[5] Takashi Iizuka,[1] Takashi Sakurai,[4] Tetsuo Noda,[5,6] Osamu Minowa,[5,6] and Katsuhisa Ikeda[1]

[1]Department of Otorhinolaryngology, Juntendo University Faculty of Medicine, Tokyo, Japan. [2]Division of Neurology, Children's Hospital of Philadelphia, Philadelphia, Pennsylvania, USA. [3]Department of Neurology, Perelman School of Medicine at the University of Pennsylvania, Philadelphia, Pennsylvania, USA. [4]Department of Cellular and Molecular Pharmacology, Juntendo University Graduate School of Medicine, Tokyo, Japan. [5]Department of Cell Biology, Japanese Foundation for Cancer Research, Cancer Institute, Tokyo, Japan. [6]Team for Advanced Development and Evaluation of Human Disease Models, RIKEN BioResource Center, Tsukuba, Japan.

Hereditary deafness affects approximately 1 in 2,000 children. Mutations in the gene encoding the cochlear gap junction protein connexin 26 (CX26) cause prelingual, nonsyndromic deafness and are responsible for as many as 50% of hereditary deafness cases in certain populations. Connexin-associated deafness is thought to be the result of defective development of auditory sensory epithelium due to connexion dysfunction. Surprisingly, CX26 deficiency is not compensated for by the closely related connexin CX30, which is abundantly expressed in the same cochlear cells. Here, using two mouse models of CX26-associated deafness, we demonstrate that disruption of the CX26-dependent gap junction plaque (GJP) is the earliest observable change during embryonic development of mice with connexin-associated deafness. Loss of CX26 resulted in a drastic reduction in the GJP area and protein level and was associated with excessive endocytosis with increased expression of caveolin 1 and caveolin 2. Furthermore, expression of deafness-associated *CX26* and *CX30* in cell culture resulted in visible disruption of GJPs and loss of function. Our results demonstrate that deafness-associated mutations in *CX26* induce the macromolecular degradation of large gap junction complexes accompanied by an increase in caveolar structures.

Introduction

Hearing loss is the most common congenital sensory deficit (1, 2). Approximately 1 child in 1,000 is affected at birth or during early childhood by severe hearing loss, which is defined as prelingual deafness (3, 4), with about half of the cases attributable to genetic causes (5). Among the more than 100 known forms of nonsyndromic deafness with identified genetic loci, by far the most common and best characterized is the one associated with *GJB2* (OMIM 121011), the gene encoding the connexin 26 (CX26) protein (6). This gap junction protein, which assembles to form channels between cells in the cochlear supporting cells, allows the rapid removal of K^+ away from the base of hair cells, resulting in the recycling of this ion back to the endolymph to maintain cochlear homeostasis (7). CX26 and CX30 are the two most abundantly expressed gap junction proteins in the cochlea (8) and form heteromeric and heterotypic channels in most of the cochlear gap junction plaques (GJPs) (9) as well as in in vitro experiments (10). In addition to their effects on K^+, gap junction proteins mediate the movement of Ca^{2+} and anions via inositol 1,4,5-trisphosphate, as well as the cell-signaling, nutrient, and energy molecules ATP and cAMP (11).

Connexins are assembled into hexameric connexons in the endoplasmic reticulum and are trafficked to the plasma membrane. Hemichannels dock head to head with partner hexameric channels positioned on neighboring cells (12). The resulting GJP may vary from 100 nm to several micrometers in diameter and can contain up to 10,000 connexons. Newly synthesized gap junctions always merge into the outside of existing GJPs, and the older gap junctions in the central area of the plaques are internalized in approximately 1 to 5 hours (13). Different types of connexin channels segregate into the different plaques forming both hetero- and homoconnexons (14). This dynamic process regulates gap junction assembly and disassembly in living cells.

In this study, we demonstrate that a mutation in CX26 induces the macromolecular degradation of large gap junction complexes accompanied by an increase in caveolar structures and that the assembly of this macromolecular complex requires CX26.

Results

In this study, we performed a detailed compositional analysis of cochlear GJPs using models of two major types of CX26-related hearing loss. The first model consists of a mouse that expresses human CX26 with the R75W dominant-negative mutation (*CX26*$^{R75W+}$; refs. 15–17 and Supplemental Figure 1, A and B; supplemental material available online with this article; doi:10.1172/JCI67621DS1). The other is a newly developed conditional *Cx26*-deficient mouse (*Cx26*$^{f/f}$ *P0-Cre*) with localized gene deletion in the inner ear under the control of the protein 0 (*P0*) promoter (ref. 18 and Supplemental Figure 1C). To confirm the expression pattern of P0 in the inner ear lineage, P0-Cre mice were crossed with R26R^{GFP} reporter mice, which contain GFP knocked into the *ROSA26* locus, allowing for the activation of GFP using Cre recombinase, and GFP signals were observed at the otocyst (Supplemental Figure 2). *Cx26*$^{f/f}$ *P0-Cre* mice had severe sensorineural hearing loss (Supplemental Figure 1D), although no abnormalities were observed in other organs (data not shown). Furthermore, these mice displayed an impaired ability to propagate Ca^{2+} oscillations from cell to cell at P5 (Supplemental Figure 3), which is probably related to an impaired function of gap junctions (19, 20) and

Conflict of interest: The authors have declared that no conflict of interest exists.
Citation for this article: *J Clin Invest.* 2014;124(4):1598–1607. doi:10.1172/JCI67621.

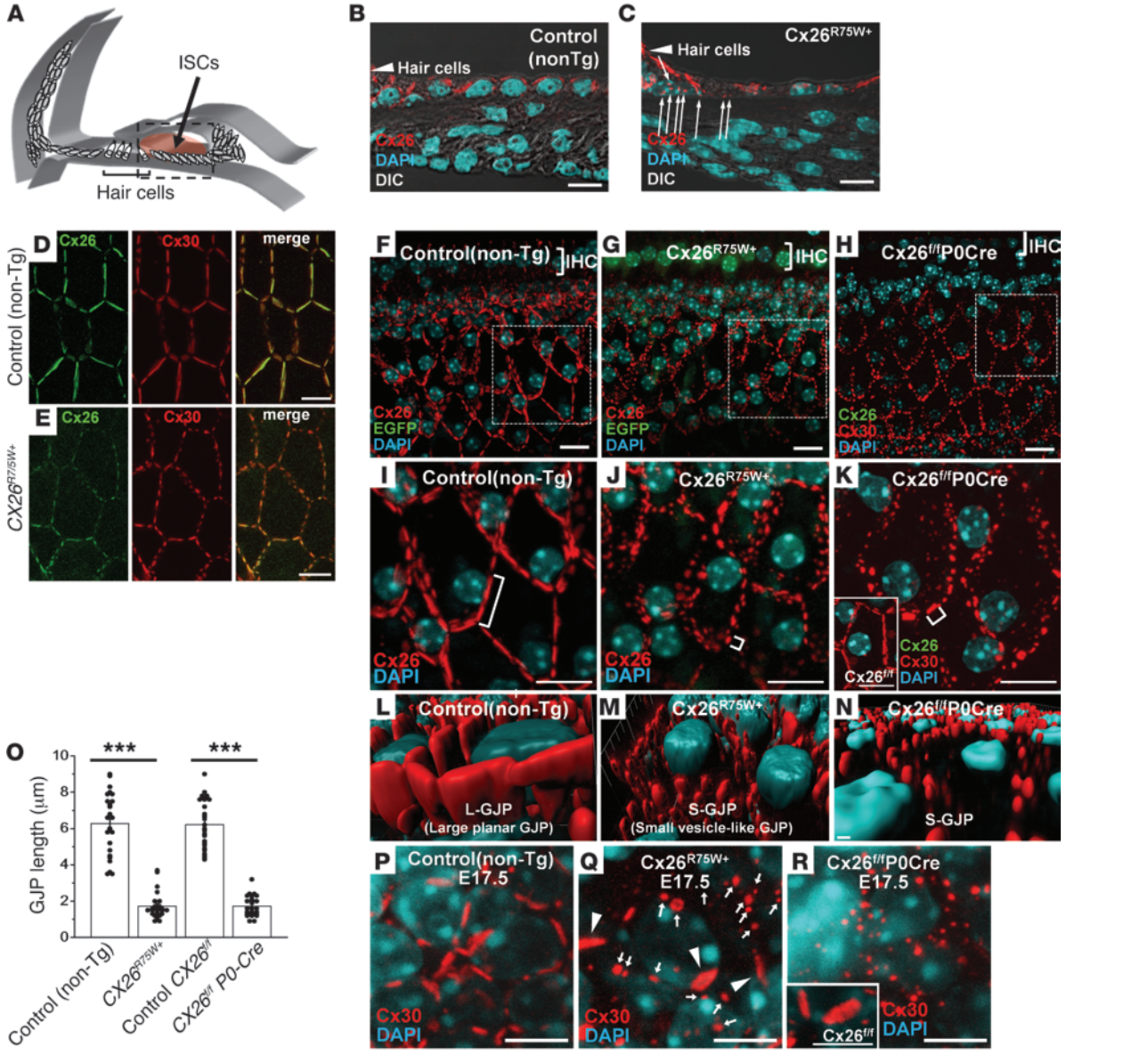

Figure 1

Drastic disruption of cochlear GJPs in two models of CX26-associated deafness. (**A**) Schematic illustration of cochlear ISCs. (**B** and **C**) CX26 distribution (in red) in ISCs (boxed region in **A**) in P12 cochlear cryosections from *CX26*$^{R75W+}$ mice show fragmented GJPs (**C**, small arrows) in contrast to GJPs in control mice (**B**). (**D** and **E**) Double staining of CX26 and CX30 in whole-mount cochlear tissue at 3 weeks showing that these GJPs are composed of both connexins in control (**D**) and *CX26*$^{R75W+}$ (**E**) mice. (**F**–**H**) GJP formation in 8-week-old adult cochleae from a *CX26*$^{R75W+}$ mouse (**G**), a non-Tg littermate control (**F**), and a *Cx26*$^{f/f}$ *P0-Cre* mouse (**H**). The partial EGFP signals in **G** indicate that it is a transgenic animal. (**I**–**K**) Image of each boxed region in **F**–**H**, respectively. Inset in **K** shows the GJPs in a *Cx26*$^{f/f}$ littermate control mouse. (**L**–**N**) Three-dimensional images reconstructed from the images in **I**–**K**, respectively. (**O**) Lengths of the largest GJPs (brackets in **I**–**K**) along a single cell border (mean ± SE, $n = 25$ for all four groups). ***$P = 4.7 \times 10^{-14}$ and 1.2×10^{-16} for *CX26*$^{R75W+}$ and *Cx26*$^{f/f}$ *P0-Cre* cochleae, respectively, relative to controls (Student's *t* test). (**P**–**R**) At E17.5, *CXx26*$^{R75W+}$ ISCs showed a number of S-GJPs (**Q**, arrows), including some L-GJPs (**Q**, arrowheads), as observed in the non-Tg control ISCs (**P**). *Cx26*$^{f/f}$ *P0-Cre* ISCs (**R**) showed totally disrupted GJPs, although the control ISCs (*Cx26*$^{f/f}$, inset in **R**) showed L-GJPs. Nuclei were counterstained with DAPI (blue). Scale bars: 10 μm.

which occurs before the onset of hearing. We note that although the propagation range was affected, the frequency of the Ca^{2+} oscillations did not change significantly (Supplemental Figure 3 and Supplemental Videos 4–7).

In a detailed analysis with a three-dimensional graphic construction of the GJP structure in the inner sulcus cells (ISCs; Figure 1A), WT adult mouse cochleae showed large, planar GJPs (L-GJPs; Figure 1I) at the cell border that formed orderly pentagonal or hexagonal outlines around normal ISCs (Figure 1, B, D, F, I, and L). In contrast, cochleae from *CX26*$^{R75W+}$ (Figure 1, C, E, G, J, M, and Supplemental Video 1) and *Cx26*$^{f/f}$ *P0-Cre* (Figure 1, H, K, and N) mice showed drastically fragmented, small vesicle–like GJPs (S-GJPs;

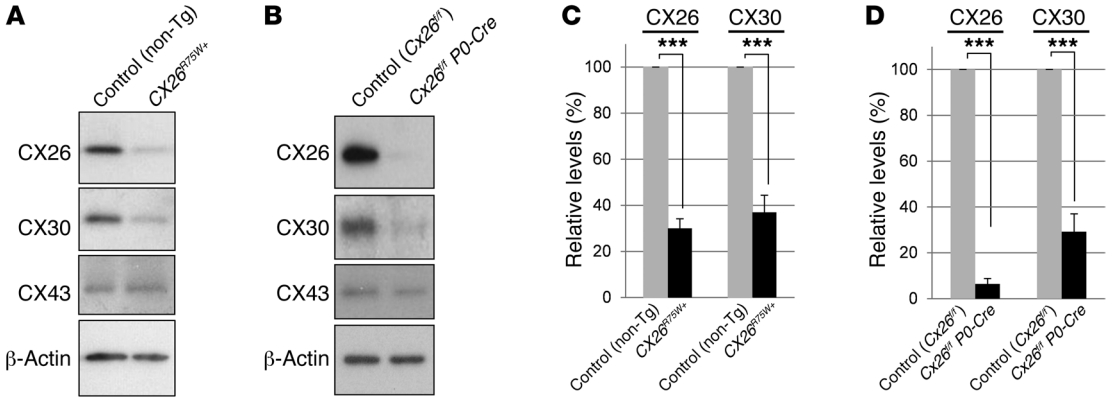

Figure 2

Changes in gap junction proteins in 8-week-old CX26-mutant mice. (**A** and **B**) Immunoblot analysis showed decreased protein expression not only for CX26, but also for CX30 in both *CX26*$^{R75W+}$ (**A**) and *Cx26*$^{f/f}$ *P0-Cre* (**B**) mice. CX43 expression in the different cochlear cells was analyzed as a control. (**C** and **D**) CX26 and CX30 protein levels were normalized to the corresponding β-actin levels and were expressed relative to the amount present in each littermate control. Values represent the mean ± SEM (error bars; $n = 5$). $P = 7.0 \times 10^{-8}$ and 1.4×10^{-5} for CX26 and CX30, respectively, in *CX26*$^{R75W+}$ mice; $P = 5.6 \times 10^{-11}$ and 8.7×10^{-6} for CX26 and CX30, respectively, in *Cx26*$^{f/f}$ *P0-Cre* mice. ***$P < 0.001$.

Figure 1, J, K, M, and N), resulting in an extremely diminished total plaque area as compared with that seen in control mice. In addition, the significant reduction in the protein levels of not only CX26 but also CX30 (Figure 2) suggested that the macromolecular complex had been degraded. The drastically dispersed plaques were observed from E17.5 (Figure 1, P–R). At the initial stage of cochlear GJP formation on E14.5, we observed that GJP disruption was already present. Two CX26-mutant mice did not show GJPs at many of the cell borders, although a part of the cells showed significantly shorter GJPs compared with the those of controls (Supplemental Figure 4). Since drastic GJP disruptions were observed even at E17.5 and the initial GJP formations were also abnormal at E14.5, which is the earliest histological change in this disease yet reported, we believe that this may be an initial phenotypic change that is followed by physiological disorder in the inner ear. As some undisrupted L-GJPs (Figure 1Q, arrowheads) were still present among the S-GJPs (Figure 1Q, arrows) in *CX26*$^{R75W+}$ mice at E17.5, GJP disruption was thought to begin during embryonic development.

Since CX26 immunolabeling was rarely detected even in *Cx26*$^{f/f}$ *P0-Cre* mouse cochlea, the numbers of CX26-positive ISCs in 5 mice were counted at the middle turn of the cochlea. Approximately 1.6% (1.6 ± 0.3%, $n = 5$) of ISCs in *Cx26*$^{f/f}$ *P0-Cre* mice showed CX26 expression (Figure 3A, arrows), in contrast to 100% (100 ± 0%, $n = 5$) in their littermate controls (*Cx26*$^{flox/flox}$, referred to herein as *Cx26*$^{f/f}$). These CX26-positive cells in *Cx26*$^{f/f}$ *P0-Cre* mice may have invaded the cochlea from other tissues such as bone marrow and thus did not undergo Cre recombinase regulation (21). This cellular mosaicism enabled us to analyze differences in the cochlear GJPs formed by adjacent cells with and without the expression of CX26 and, critically, revealed the CX26-dependent differences in the formation of the two GJP types (L-GJP and S-GJP). Cochlear GJPs with both CX26 and CX30 formed L-GJPs, as compared with the S-GJPs that formed without CX26 (Figure 3, A–E, Supplemental Figure 5, E and F, and Supplemental Videos 2 and 3). Even in a single cell, the GJP type at each junctional side varied depending on the connexin expression in the adjacent cells (Figure 3D, arrowheads). The cells were classified as either CX26-positive cells (CX26 in Figure 3, B and C), which expressed CX26 in at least one GJP at the lateral cell junction site, or CX26-negative cells (KO in Figure 3, B and C). Based on this finding, we categorized the resulting GJPs as one of four types (Figure 3, F–I). It is notable that even though a cell expressed CX26, this protein was not able to assemble into a GJP when the adjacent cell did not also express CX26 (Figure 3H).

These GJP disruptions in the cochlea were also produced by human cDNA clones in HeLa cells (22, 23) that stably expressed mutant CX26 together with CX30 (Figure 4, A–E). Interestingly, these cell lines clearly showed functional differences in neurobiotin (NB) transfer analysis (Figure 4, I, J, O, and P) depending on the level of GJP disruption (Figure 4, F, G, L, and M), even when mutations at the same amino acid in CX26 were used (i.e., R75W and R75Q, which also cause hereditary deafness; ref. 24). The cells with smaller GJPs had less extensive NB dye transfer as compared with cells with larger GJPs (Figure 4, H–Q). To investigate whether supplementation with WT CX26 can rescue the GJP size in the two mutant mouse strains, we performed an overexpression experiment with adeno-associated virus (AAV) carrying WT CX26 tagged with FLAG in cochlear organ cultures from *CX26*$^{R75W+}$ mice and *Cx26*$^{f/f}$ *P0-Cre* mice (Supplemental Figure 6). In this context, CX26-FLAG formed mainly small (0.93 ± 0.14 μm) vesicle-like GJPs in *CX26*$^{R75W+}$ mouse cochleae, although it formed relatively large (3.7 ± 0.7 μm) GJPs in cochleae from *Cx26*$^{f/f}$ *P0-Cre* mice. Considering the original GJP size for the adult CX26-mutant mice shown in Figure 1O (~1 μm for both CX26-mutant mice and ~6 μm for the control littermate), the GJP size of *Cx26*$^{f/f}$ *P0-Cre* ISCs may be rescued by supplementation with WT CX26, while some mutants such as CX26R75W^{+} may not be rescued due to their dominant-negative effects. These results corresponded with the functional changes analyzed by fluorescence recovery after photobleaching (FRAP) or dye transfer analysis in HeLa cells in our previous reports (22, 23).

After extensive protein analysis with mutant cochleae (Supplemental Figure 7 and data not shown), we found that caveolin 1 (CAV1) and caveolin 2 (CAV2), components of the caveolae (which form during endocytosis), were molecules that were altered in the pathology. Interestingly, we observed a drastic isoform shift in CAV1 from CAV1α to CAV1β, which lacks the N-terminal

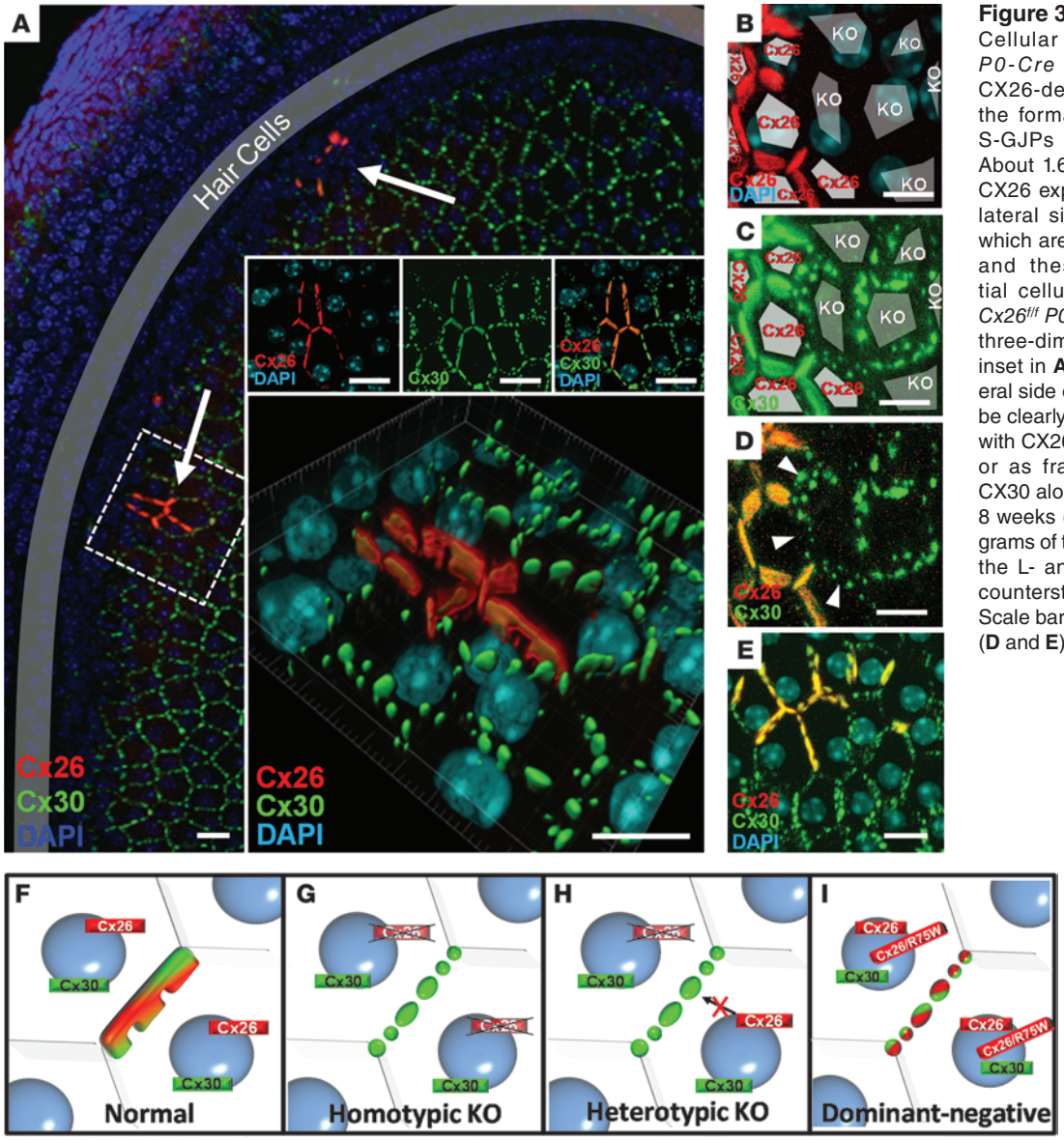

Figure 3
Cellular mosaicism in *Cx26$^{f/f}$ P0-Cre* mice revealed the CX26-dependent differences in the formation of L-GJPs versus S-GJPs shown in Figure 1. (**A**) About 1.6 % of the ISCs showed CX26 expression on at least one lateral side (arrows and insets, which are from the boxed region), and these cells showed partial cellular mosaicism in adult *Cx26$^{f/f}$ P0-Cre* mice. Confocal and three-dimensional images (large inset in **A**) revealed that each lateral side of the cell junctions could be clearly distinguished as L-GJPs with CX26 (red) and CX30 (green) or as fragmented S-GJPs with CX30 alone at 3 weeks (**A**–**D**) and 8 weeks (**E**). (**F**–**I**) Schematic diagrams of the rules used to organize the L- and S-GJPs. Nuclei were counterstained with DAPI (blue). Scale bars: 5 μm (**A**–**C**) and 10 μm (**D** and **E**).

hydrophilic region of CAV1α in *CX26^{R75W+}* cochleae, and found significantly increased expression of CAV1β and CAV2 in both *CX26^{R75W+}* and *Cx26$^{f/f}$ P0-Cre* cochleae (Figure 5, A–D). CAV1 and CAV2 showed excessive accumulation (Figure 5, E–K) in 3-week-old *CX26^{R75W+}* cochleae. These cells that accumulated CAV1 or CAV2 were occasionally observed at the inter-GJP space or on the surface of the GJPs (Figure 5, G, H, J, and K) in 3-week-old *CX26^{R75W+}* cochleae, although no accumulated signals were observed in the control mice (Figure 5, E and I). We quantified the number of ISCs that had accumulated CAV1 and CAV2 in both CX26 mutants. There was no difference in their distribution pattern or in the number of positive cells (P = 0.16) with respect to CAV1 (7.3 ± 1.3%) and CAV2 (5.6 ± 0.9%) accumulation (Figure 5L). In the overexpression of CAV1β with WT CX26, CX26R75W, and CX30 in HEK293 cells, we observed that numerous GJPs at the cell borders and the connexin vesicles were accompanied by accumulated CAV1β, although WT CX26 with CAV1β did not show such a distribution pattern (Supplemental Figure 8). We also observed numerous CAV1- and CAV2-positive vesicles at the S-GJPs in the two mutant mice in the adult stage as compared with those seen at the L-GJPs in the control mice (Figure 5, M and N). These changes were associated with an increase in the caveolar structures (Figure 6, B and E–K) that are indicative of endocytosis, which leads to membrane retrieval and, perhaps, abnormal GJP formation.

Based on electron microscopic analysis of the ISCs, we observed that both *CX26^{R75W+}* and *Cx26$^{f/f}$ P0-Cre* mice also formed gap junctions, although there were a number of discontinuous gap junctions (Figure 6, B, D, and K) with excessive endocytosis (Figure 6, B, E, F, and G–K) or abnormally condensed intermembrane layers (Figure 6, E and F) around the gap junctions in *Cx26$^{f/f}$ P0-Cre* mice. In contrast with their littermate controls (Figure 6, A and C), significantly larger numbers of caveolae and vesicles were detected at cell borders in both *CX26^{R75W+}* mice and *Cx26$^{f/f}$ P0-Cre* mice (Figure 6L). The distributions and the number of caveolae were nearly identical between both types of mutant mice and were consistent with the immunolabeling for CAV1 and CAV2 around GJPs (Fig-

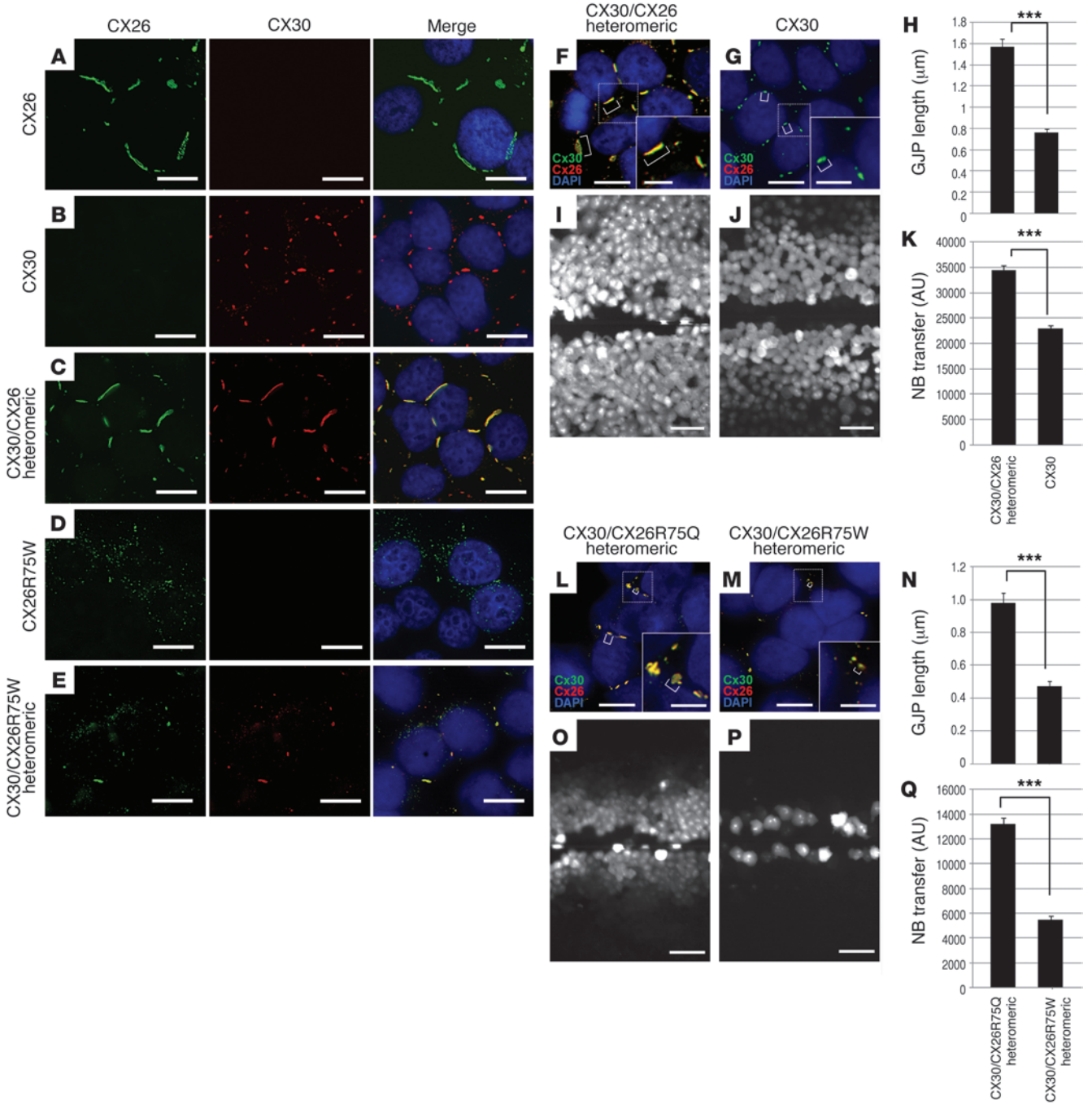

Figure 4

Disruption of cochlear GJPs is reproduced by human cDNA clones for CX30 and CX26, with or without mutations in HeLa cells, and leads to functional differences in dye transfer depending on the resultant GJP sizes. (**A**–**E**) Clear differences in GJP formation were observed in HeLa cells that expressed the indicated connexin(s), which made homomeric or heteromeric channels. Cells were colabeled with anti-CX26 (green) and anti-CX30 (red) antibodies and were counterstained with DAPI (blue). L-GJPs were observed only when normal CX26 was expressed alone (**A**) or was coexpressed with CX30 (**C**). The other combinations (**B**, **D**, and **E**) formed S-GJPs. (**F**–**Q**) In HeLa cells that expressed CX30 and CX26, cells with smaller GJPs demonstrated decreased NB transfer. (**F**, **G**, **L**, and **M**) Shown are HeLa cells that expressed WT CX30 alone (CX30) or coexpressed WT CX30 and WT CX26 (CX30/CX26), or the indicated CX26 mutants (CX30/Cx26R75Q or CX30/CX26R75W). CX26 and CX30 were colocalized, and the GJP size differed across cell lines. (**H** and **N**) Quantitative analysis of the GJP length (mean ± SEM). $^{***}P = 3.3 \times 10^{-17}$ (**H**) or $P = 7.7 \times 10^{-12}$ (**N**). (**I**, **J**, **O**, and **P**) Digital fluorescence images of HeLa cells expressing the indicated connexin(s) after NB scrape-loading. (**K** and **Q**) Quantitative analysis of intercellular NB transfer after scrape-loading. Columns represent the mean distance (± SEM) of NB transfer from the scrape line. $^{***}P = 9.6 \times 10^{-9}$ (**K**) or $P = 3.2 \times 10^{-11}$ (**Q**). Scale bars: 10 μm and 5 μm (insets).

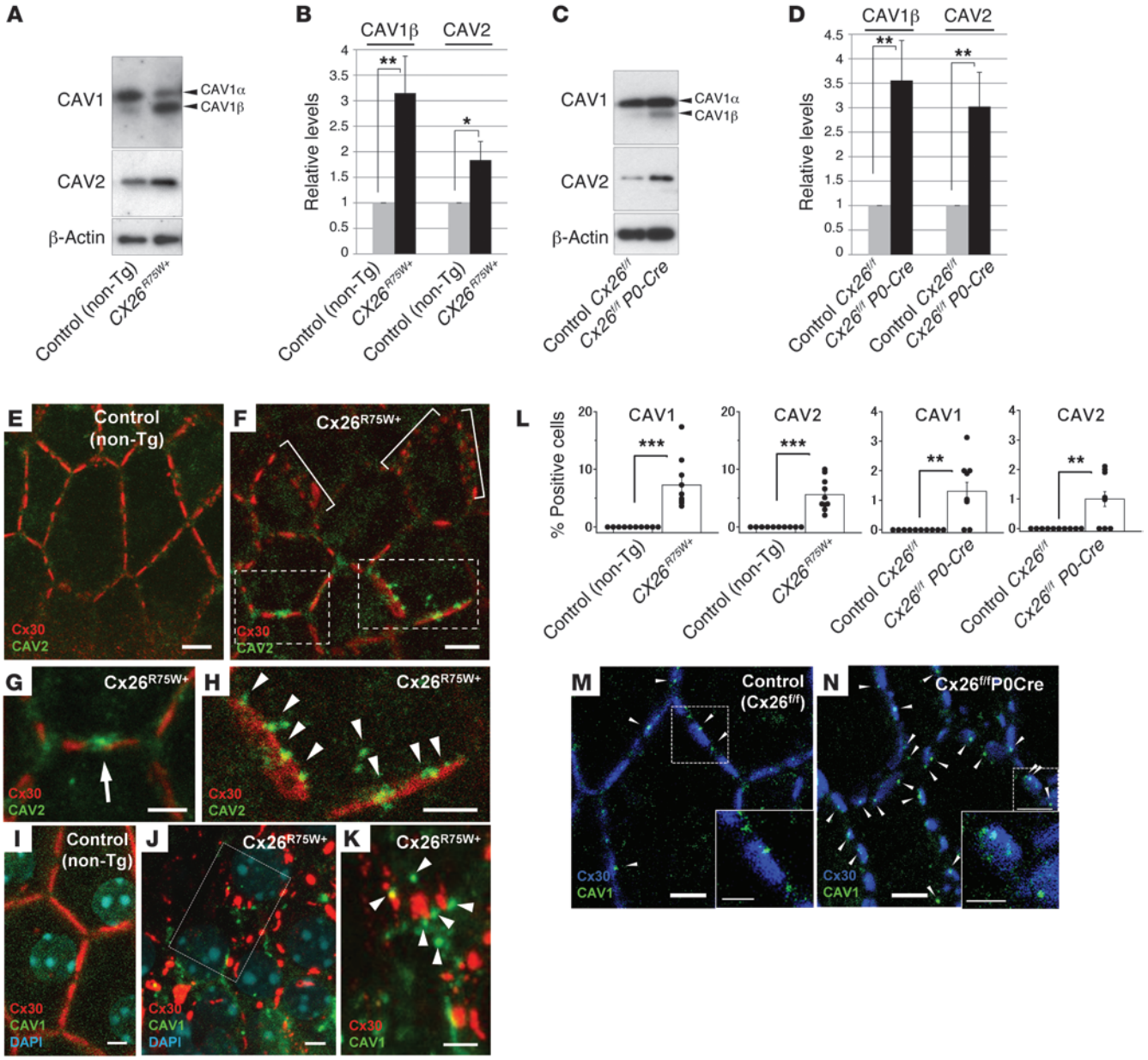

Figure 5

Changes in the endocytosis proteins CAV1 and CAV2 in CX26-mutant mouse cochlea. The CAV1 isoform preference shifted from α to β in *CX26^{R75W+}* cochlea (**A**). The CAV1β and CAV2 increased in both mutant mice (**A** and **C**) at 8 weeks of age, as shown by Western blotting. Protein levels of CAV1β (**B**) and CAV2 (**D**) are expressed relative to the amount present in each littermate control (mean ± SEM, $n = 5$). $P = 0.009$ and 0.03 for CAV1β and CAV2, respectively, in *CX26^{R75W+}* cochlea. $P = 0.007$ and 0.01 for CAV1β and CAV2, respectively, in *Cx26$^{f/f}$ P0-Cre* cochlea. (**E**–**K**) Accumulation of CAV2 and CAV1 in 3-week-old non-Tg littermate controls (**E** and **I**) and *CX26^{R75W+}* mice (**F**–**H**, **J**, and **K**) with S-GJPs (brackets in **F**) was occasionally observed at the inter-GJP space (**G**, arrow) and on the surface of the GJPs (**H**, arrowheads), differing from that seen in littermate controls (**I** and **E**). The boxed regions in **F** and **J** are magnified in **G**, **H**, and **K**, respectively. (**L**) Numbers of cells with accumulated CAV1 or CAV2 were counted in five animals from each group (mean ± SEM, $n = 10$; $P = 0.0003$, 6.1×10^{-5}, 0.001 and 0.002, from left to right). (**M**–**N**) In adult mice, vesicles positive for CAV1 (arrowheads) were frequently detected on GJPs in *Cx26$^{f/f}$ P0-Cre* mice (**K**), but not in their littermate controls (**J**). Boxed regions are magnified in the bottom right corner. Scale bars: 10 μm and 5 μm (insets). $^*P < 0.05$; $^{**}P < 0.01$; $^{***}P < 0.001$.

ure 5, M and N) and the upregulation of the caveolin proteins (Figure 5, A–D). This may be associated with the membrane retrieval (Figure 6K) caused by excessive endocytosis and the formation of abnormal GJPs. In the labeling with cholera toxin subunit B (CTxB), it was shown that GJPs with CX26 and CX30 did not colocalize with lipid rafts in control mice (Supplemental Figure 9, A, C, and E). In contrast, the lipid raft signals in *Cx26$^{f/f}$ P0-Cre* mice localized between S-GJPs with no regularity and with more diffuse labeling and less clarity as compared with those in control mice (Supplemental Figure 9, B, D, and F).

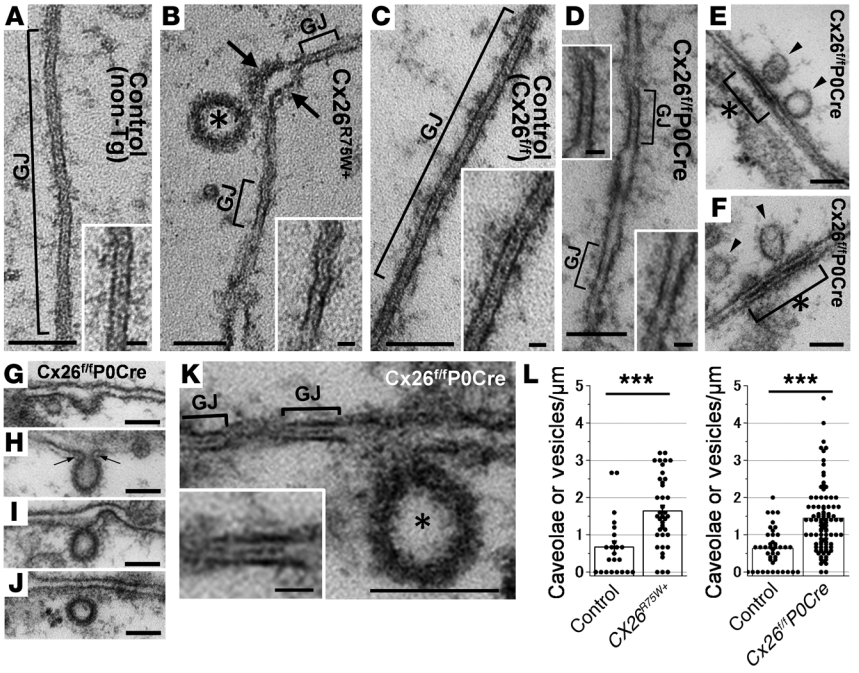

Figure 6

Discontinuous gap junctions with excessive endocytosis in CX26-mutant mice. (**A**–**K**) Ultrastructure of gap junctions and caveolae in 5-week-old *CX26^{R75W+}* (**B**) and *Cx26$^{f/f}$ P0-Cre* (**D**–**K**) mice compared with their respective littermate controls (**A** and **C**). Horizontal ultrathin sections of ISCs revealed that most of the gap junctions (GJs, brackets) were remarkably shorter or discontinuous (**B**, **D**, and **K**) compared with those of the control ISCs (**A** and **C**). (**B**) A caveolar vesicle (asterisk) with dissociated plasma membrane (arrows) around a short gap junction in a *CX26^{R75W+}* mouse. In both mutant mice, numerous caveolae and vesicles (**B** and **K**, asterisks; **E** and **F**, arrowheads; **G**–**J**) were observed. (**E** and **F**) Abnormally condensed intermembrane layers (asterisks with brackets) at the cell borders were observed in *Cx26$^{f/f}$ P0-Cre* mice. (**G**–**J**) In *Cx26$^{f/f}$ P0-Cre* mice, the plasma membrane showed a small cave-like shape (**G**), an invagination with a neck (**H**, arrows), and the formation of a vesicle-like structure (**I**); the vesicle was separated from the plasma membrane (**J**). (**K**) A caveolar vesicle (asterisk) is shown at the edge of discontinuous short gap junctions (inset) with clear internal layers. (**L**) Number of caveolae or caveolar vesicles that were counted around each cell border (mean ± SEM with dot plots): n = 23 and 39 cells for the littermate control and *CX26^{R75W+}* mice, respectively (***$P = 3.2 \times 10^{-5}$); n = 42 and 97 for the littermate control and *Cx26$^{f/f}$ P0-Cre* mice, respectively (***$P = 8.4 \times 10^{-10}$). Scale bars: 100 nm and 20 nm (insets).

With regard to this drastic GJP disruption, we hypothesized that the abnormal GJPs in both CX26-mutant mice populations were triggered by abnormalities in the formation of the protein complex associated with CX26 and that the resultant molecular changes could lead to the disruption of GJP formation. As for internalization of CX26 protein, we fractionated the cochlear proteins and analyzed them by immunoblotting. CX26 from CX26R75W$^+$ mice was, however, distributed in the plasma membrane fraction, as was CX26 from the control mice (Supplemental Figure 10A). To determine the affinity for other connexins or connexons, we performed coimmunoprecipitation using CX26 antibodies. CX30 was detected in both the CX26R75W$^+$ mice and control mice, and thus no substantive abnormality in the CX26-CX30 interaction in the macromolecular complex could be demonstrated (Supplemental Figure 10B). To examine the interactions with the cytoskeleton, we performed several in vitro experiments with cytochalasin D treatment, which destroys the cytoskeleton, in HEK cells transfected with CX26-EGFP with or without the R75W mutation. We did not, however, observe an effect on GJP formation resulting from disruption of the cytoskeleton (data not shown). As for ubiquitination and autophagy of the GJP, including CX26, we examined the association of ubiquitination and autophagy with GJP disruption in CX26 mutants by immunoblot analysis and transmission electron microscopy. We could not find convincing evidence to show that these processes were more prevalent in CX26-mutant cochleae than in control cochleae (data not shown). As for membrane retrieval at cell junctions, our ultrastructural pathology demonstrated that a significantly larger number of caveolae and vesicles were associated with the cell border (including small gap junctions) in *Cx26$^{f/f}$ P0-Cre* mice as compared with those in the control mice (Figure 6). This may indicate that excessive endocytosis occurs in the presence of this CX26 mutation, leading to membrane retrieval that may accelerate GJP degradation.

Discussion

In this study, we demonstrated a novel molecular pathology in the cochlea, that of degradation of the gap junction macromolecular complex in CX26-associated deafness, as well as a novel mechanism of GJP formation into one of two types (L-GJPs or S-GJPs) that is dependent on CX26 expression. These findings were consistent not only in cochlear cells, but also in a human cell line with artificial connexin expression. Our data suggest that both the dominant-negative R75W mutation and the absence of CX26 affect the accumulation and assembly of gap junction units in the cell-cell junctions between cochlear supporting cells.

Regarding the initial phenotype of the hearing organ in the connexin mutants (Figure 1 and Supplemental Figure 4), we have previously described an early histological change in CX26-mutant mice, which showed an absence of the small space needed to form the future tunnel of Corti around P5 (15). As for hearing function, the earliest change detected by the auditory brainstem response occurs only after P11 (15), because hearing input to the mouse cochlea normally begins between P11 and P12 (25). With respect to the function of the cochlear gap junction, Ca^{2+} responses fail to propagate in organotypic cultures with defective expression of CX26 or CX30 from P3 through P6 (26). Thus, to the best of our knowledge, the phenotype at the embryonic stage shown in the present study (Figure 1 and Supplemental Figure 4) has not been previously reported.

The mosaicism generated by our newly developed *Cx26$^{f/f}$ P0-Cre* mice revealed that the formation of L-GJPs versus S-GJPs critically depended on CX26 expression, and CX26 expression from both adjacent cells was essential to form normal L-GJPs — even if CX30 was highly expressed in the same cells (Figure 1, D and E). The in vivo (Figure 3) and in vitro (Figure 4) findings concerning GJP formation provided conclusive evidence demonstrating that the formation of

L-GJPs has a definite CX26 dependency and that CX26 is required to form the large macromolecular complex of gap junctions.

Regarding the association between connexins and caveolins (Figure 5 and Supplemental Figure 9), gap junction activity is regulated by protein kinase Cγ activity associated with CAV1-containing lipid rafts (27). Connexin family members (including CX26) are targeted to lipid raft domains, where they interact directly with caveolins such as CAV1 (28). Interestingly, in that experimental system, CX26 was targeted to lipid rafts only when CX26 was coexpressed with CAV1, suggesting that CAV1 recruits CX26 to lipid rafts, although other connexins such as CX32, CX36, CX43, and CX46 showed this lipid raft targeting without any artificial expression of CAV1 (28). These data showing that CX26 is excluded from the lipid raft fraction are in agreement with our present observation that the lipid raft signals in *Cx26$^{f/f}$ P0-Cre* mice localized between S-GJPs with no regularity and with more diffuse labeling and less clarity compared with those in control mice (Supplemental Figure 9). This suggests that the partial targeting to lipid rafts of connexins such as CX30 occurred to prevent the assembly or reassembly of GJPs in CX26-mutant mice.

In many tissues, CX26 is often coexpressed with another connexin in individual cells (29), and it can form heterotypic channels containing homomeric or heteromeric channels with CX30 (10). Hearing loss caused by CX30 deficiency in mice is rescued by the overexpression of CX26 (30). This observation demonstrates that CX26 can compensate for CX30. In contrast, when CX26 is absent in conditional CX26-null mice, CX30 overexpression does not rescue the severe hearing loss (31). Thus, it was concluded that CX26 plays an essential role in the development of the auditory sensory epithelium and that its unique developmental functions required for normal hearing cannot be replaced by CX30 (31). In lens fiber cells, although the expression of CX46 and CX50 overlap extensively, mice that lack one or the other of these connexins (and that serve as a model system for cataract formation) exhibit different phenotypes (32, 33). Macromolecular complex degradation in GJPs that affects other partner connexins and critically reduces functional plaque area may explain not only hearing loss, but also conditions such as cataracts resulting from gap junction dysfunctions with uncompensated connexin mutations.

Until now, hereditary deafness with connexin mutations was believed to be initiated by a single molecular dysfunction or dominant-negative effect on the connexin partners (34), and the primary pathology had never been observed at the embryonic stage. As for the cell degeneration in the connexin mutants, Liang et al. reported that cell degeneration was not a primary cause of CX26 deficiency–associated hearing loss (35). Using a CX26-deficient mouse model similar to the one used in the present study, they demonstrated that cochlear cells, including spiral ganglion neurons, had no significant degeneration throughout postnatal development, although auditory brainstem responses (ABRs) were absent in the whole frequency range (8–40 kHz) after birth.

Here, we demonstrate that connexin-associated deafness, which is the most frequent type of hereditary deafness, may be initiated not by a single molecular dysfunction of connexins, but by a macromolecular complex degradation of GJPs from the embryonic stage. This loss of GJP area may then abolish the proper ionic gradient needed for intercellular communication in the cochlea.

To the best of our knowledge, this is the first report demonstrating that a mutation in CX26 induces macromolecular degradation of large gap junction complexes accompanied by an increase in caveolar structures, which may lead to excessive membrane retrieval and result in a drastic reduction in the GJP area. This may represent a new molecular pathology for hereditary sensorineural deafness and for the general formation of gap junctions, and thus this machinery could be an effective target for drug design and chemical screening to reinforce the assembly of the other cochlear connexins such as CX30.

Methods

Dominant-negative CX26R75W (CX26^{R75W+}) transgenic mice. *CX26^{R75W+}* mice were obtained from a breeding colony of a previously reported line (16). *CX26^{R75W+}* mice were maintained on a C57BL/6J background and crossed with C57BL/6J animals to generate R75W transgenic offspring. Nontransgenic (non-Tg) littermates on a C57Bl/6J background were always used as the control for *CX26^{R75W+}* mice.

Generation of novel conditional knockout mouse for CX26. A targeting vector of a floxed *Cx26* allele including exons 1 and 2 was constructed using phage DNA clones from a genomic library of J1 ES cells. An approximately 8.4-kb HindIII-BamHI fragment with exon 1 and a 2.85-kb SacI-SacI fragment containing the 3′ half of exon 2 were isolated and used to construct a targeting vector with long and short homologous sequences, respectively. One loxP sequence was introduced at the end of intron 1, and a Neo cassette was introduced between two loxP sequences in exon 2. The diphtheria toxin A (DT-A) chain expression cassette was used as a negative selection marker. The linearized targeting vector was introduced into J1 ES cells by electroporation, and G418-resistant clones were analyzed by Southern blotting to isolate the homologous recombinant as described (18, 36). Identified recombinant ES cells were injected into C57/BL6J blastocysts. A mouse strain harboring the floxed *Cx26* allele was established by crossing chimeras with C57/BL6J females to produce F1 heterozygotes (*Cx26$^{flox/+}$*). F2 offspring were generated by crossing F1 heterozygotes, and their genotyping was performed by PCR amplification. No apparent abnormalities were detected in the *Cx26$^{f/f}$* mice. Otic vesicle–specific CX26-knockout mice were generated by breeding *Cx26$^{f/f}$* mice with mice that expressed the Cre recombinase gene under the control of the promoter of the *P0* gene (*P0-Cre* mice, on a C57BL/6J background), as described (18). To evaluate Cre recombinase expression and distribution, P0-Cre mice were crossed with ROSA26-GFP reporter mice (Gt-ROSA-26sortm1sor, R26R), and the four mice from two litters were analyzed by fluorescence and confocal microscopy (Supplemental Figure 2). *Cx26$^{f/f}$* on a C57Bl/6J background in the littermates was always used as the control for the *Cx26$^{f/f}$ P0-Cre* mice.

Immunohistochemistry. Mice were anesthetized, killed, and the inner ear tissues were removed. The cochleae were further dissected and fixed in 4% PFA. Immunofluorescence staining with antibodies against CX26 (rabbit IgG from Life Technologies and mouse IgG from LifeSpan Biosciences), CX30 (rabbit IgG; Life Technologies), caveolin 1 (mouse IgG; BD Biosciences), and caveolin 2 (mouse IgG; BD Biosciences) was performed on whole-mount preparations of the finely dissected organ of Corti or cochlear cryosections (5-μm) that included ISCs. We incubated the tissues in the antibody solutions for 1 hour after blocking. The following secondary antibodies were used: Cy3-conjugated anti-rabbit IgG (Sigma-Aldrich) for anti-CX26 or -CX30 rabbit antibodies; Alexa Fluor 488–conjugated anti-mouse IgG (Life Technologies) for anti-CX26 mouse antibodies; Alexa Fluor 594–conjugated anti-mouse IgG (Life Technologies) for anti-CAV1 or -CAV2 mouse antibodies; and Alexa Fluor 633–conjugated anti-rabbit IgG (Life Technologies) for CX30 in double or triple staining. Lipid rafts were visualized with Alexa Flour 594–conjugated cholera toxin subunit B (CTxB, Life Technologies). Fluorescence confocal images were obtained with an LSM510-META confocal microscope (Zeiss). Some of the green fluorescence in *CX26^{R75W+}* mice indicates the pseudocolor obtained from

the Alexa Fluor 633–conjugated secondary antibody signal (Life Technologies), because these mice have ubiquitous EGFP expression from their transgene. *z*-stacks of images were collected at 0.5-μm intervals, and the single image stacks were constructed with the LSM Image Browser (Zeiss); three-dimensional images and videos were constructed using IMARIS software (Bitplane). We analyzed at least five samples from five animals at each age used, and representative images are shown. The compared images were photographed and processed using identical parameters. Three-dimensional images were constructed with *z*-stacked confocal images by IMARIS (Bitplane). Quantitative analysis of the GJP length (mean ± SEM) was performed with the LSM Image Browser (Zeiss), and data were compared using a Student's *t* test (Microsoft Excel).

Western blot analysis. The mouse cochlear proteins were extracted with T-PER Tissue Protein Extraction Reagent (Thermo Scientific) from at least six cochleae that included the organ of Corti, lateral wall, and stria vascularis. The proteins were resolved by SDS-PAGE with 4% to 20% mini-PROTEAN TGX gels (Bio-Rad Laboratories) and then transferred onto a PVDF membrane (Amersham Hybond-P; GE Healthcare). After blocking, the membranes were processed through sequential incubations with anti–caveolin 1 (1:1,000; BD) and anti–caveolin 2 (1:500; Sigma-Aldrich), rabbit anti-CX26 (1:1,000; Life Technologies), mouse anti-CX26 (1:1,000; Life-Span Biosciences), and monoclonal anti–β-actin (1:1,500; Sigma-Aldrich) with HRP-conjugated anti-rabbit or anti-mouse IgG (1:40,000; GE Healthcare) as the secondary antibody. Amersham ELC Prime Western Blotting Detection Reagent (GE Healthcare) was then used for visualization, and the signal was developed on x-ray film (Amersham Hyperfilm ECL; GE Healthcare). Each experiment was repeated at least three times. Densitometric analysis of the band intensities was performed with ImageJ software (NIH). The data were normalized to the corresponding β-actin levels, expressed relative to the amount present in each littermate control, and compared using a Student's *t* test (Microsoft Excel).

Transmission electron microscopy. Animals were deeply anesthetized and perfused intracardially with 0.01 M PBS, followed by 2% PFA and 2% glutaraldehyde in 0.1 M cacodylate buffer. The cochleae were opened and flushed with the fixative for 2 hours at room temperature. After washing, the specimens were postfixed for 1.5 hours in 2% osmium tetroxide in 0.1 M phosphate buffer and then dehydrated through a graded ethanol series and embedded in Epon. Horizontal sections of the surface of the cochlear membrane labyrinth were cut, stained with uranyl acetate and lead citrate, and examined by electron microscopy (H-7100; Hitachi). The numbers of caveolae and vesicles were counted and compared using a Student's *t* test (Microsoft Excel).

Expression constructs and cell lines expressing CX26, CX30, or CX26 mutants. Expression constructs and cell lines were generated as previously described (10, 22). Briefly, human *GJB6* was obtained by RT-PCR (Superscript II; Life Technologies) from human corpus callosum RNA (Clontech) and subcloned into the pIRESpuro3 vector, then human *GJB2* was subcloned into the pIRESneo3 vector, and the *GJB2* mutations were introduced into the ORF of human *GJB2* cDNA by PCR site–directed mutagenesis using the QuickChange kit (Stratagene). Communication-incompetent HeLa cells were used to generate the stable cell lines expressing WT CX30. To generate cells expressing both WT CX30 and WT CX26 or CX26 mutants, one cloned cell line that stably expressed CX30 was transfected with *GJB2* in pIRESneo3. After selection with both 1 μg/ml of puromycin (Sigma-Aldrich) and 1 mg/ml of G418 (Life Technologies) for about 3 weeks, the colonies were trypsinized, and these bulk-selected cells were expanded for the subsequent studies. Quantitative analysis of GJP length (mean ± SEM) was performed with ImageJ software.

Immunocytochemistry and GJP quantification. HeLa cells were grown on coverslips for 2 days to a confluence of approximately 70% to 90%, fixed in acetone, and incubated with a monoclonal antibody (33-5800, diluted 1:500; Zymed Laboratories) and a rabbit antiserum against the C terminus of CX30 (71-2200, diluted 1:1,000; Zymed Laboratories); these did not cross-react with each other, as previously shown (10). The cells were visualized with tetramethylrhodamine isothiocyanate–conjugated (TRITC-conjugated) donkey anti-rabbit (Abcam) and FITC-conjugated donkey anti-mouse secondary antibodies (Abcam). The cells were photographed under a Leica fluorescence microscope with a Hamamatsu C4742-95 digital camera connected to a G5 Mac computer using OpenLAB 2.2 software for deconvolution. The images were analyzed for GJP length using ImageJ software. All GJPs from 30 to 35 cells of each cell line were measured, and the mean GJP length was compared between cells expressing CX30 alone and those expressing both CX30 and CX26, or between cells expressing both CX30 and CX26R75Q and those expressing both CX30 and CX26R75W, using a Student's *t* test (Stata).

Dye transfer with Scrape-loading. Dye transfer was investigated using a scrape-loading assay as previously described (10). Briefly, parental HeLa cells, bulk-selected cells that expressed WT CX30 alone, or cells that coexpressed WT CX30 and CX26 or one of the CX26 mutants (R75Q or R75W) were grown to confluence on coverslips. Following the scrape-loading with 2% NB and diffusion, the cells were washed, fixed, and the NB was visualized by TRITC-conjugated avidin (Sigma-Aldrich). Cells were photographed under a Leica fluorescence microscope with a Hamamatsu C4742-95 digital camera connected to a G5 Mac computer, using OpenLAB 2.2 software. Dye transfer was quantified by measuring the distance from the scrape line to the point where the average fluorescence intensity dropped to 1.5 times the background intensity. Eleven to twelve images were acquired from each of three different plates of cells. The images were processed and analyzed with ImageJ software, and the mean distance was calculated using Microsoft Excel software and compared using a Student's *t* test (Stata).

Statistics. A one-tailed Student's *t* test, with a significance criterion of $P < 0.05$, was used to compare the GJP length, relative protein levels, number of cells positive for accumulated caveolins, ABR thresholds, propagation ranges of Ca^{2+} signaling, distance of dye transfer, and number of caveolae or vesicles.

Study approval. All experimental protocols were approved by the IACUC of Juntendo University School of Medicine and were conducted in accordance with the NIH guidelines for the care and use of laboratory animals.

Acknowledgments

This work was supported in part by a research grant from the Ministry of Education, Science and Culture (JSPS KAKENHI 25462563, to K. Kamiya); the Ministry of Health, Labor and Welfare of Japan (to K.Kamiya); the MEXT support program for the Strategic Research Foundation at Private Universities, 2011–2012 (to K. Ikeda); the Terumo Life Science Foundation (to K. Kamiya); and by NIH grant KO8DC005394 (to S.W. Yum). We thank M. Yoshida at the Laboratory of Ultrastructure Research for help with the transmission electron microscopy; Y. Fujitani for providing the reporter mouse line; H. Mochizuki for providing the AAV; Y. Yokoyama and B. Kuerban for experimental assistance; the staff of the Division of Proteomics and Biomolecular Sciences for help with our proteomic analysis; and Y. Uchiyama for helpful advice.

Received for publication November 1, 2012, and accepted in revised form January 2, 2014.

Address correspondence to: Kazusaku Kamiya, Department of Otorhinolaryngology, Juntendo University Faculty of Medicine, Hongo 2-1-1, Bunkyo-ku, Tokyo 113-8421, Japan. Phone: 81.3.5802.1229; Fax: 81.3.5840.7103; E-mail: kkamiya@juntendo.ac.jp.

1. Chan DK, Schrijver I, Chang KW. Connexin-26-associated deafness: phenotypic variability and progression of hearing loss. *Genet Med*. 2010; 12(3):174–181.
2. Mason JA, Herrmann KR. Universal infant hearing screening by automated auditory brainstem response measurement. *Pediatrics*. 1998;101(2):221–228.
3. Petersen MB, Willems PJ. Non-syndromic, autosomal-recessive deafness. *Clin Genet*. 2006;69(5):371–392.
4. Morton NE. Genetic epidemiology of hearing impairment. *Ann N Y Acad Sci*. 1991;630:16–31.
5. Birkenhäger R, Lüblinghoff N, Prera E, Schild C, Aschendorff A, Arndt S. Autosomal dominant prelingual hearing loss with palmoplantar keratoderma syndrome: Variability in clinical expression from mutations of R75W and R75Q in the GJB2 gene. *Am J Med Genet A*. 2010;152A(7):1798–1802.
6. Kelsell DP, et al. Connexin 26 mutations in hereditary non-syndromic sensorineural deafness. *Nature*. 1997;387(6628):80–83.
7. Kikuchi T, Kimura RS, Paul DL, Takasaka T, Adams JC. Gap junction systems in the mammalian cochlea. *Brain Res Brain Res Rev*. 2000;32(1):163–166.
8. Ahmad S, Chen S, Sun J, Lin X. Connexins 26 and 30 are co-assembled to form gap junctions in the cochlea of mice. *Biochem Biophys Res Commun*. 2003;307(2):362–368.
9. Sun J, et al. Cochlear gap junctions coassembled from Cx26 and 30 show faster intercellular $Ca2^{+}$ signaling than homomeric counterparts. *Am J Physiol Cell Physiol*. 2005;288(3):C613–C623.
10. Yum SW, et al. Human connexin26 and connexin30 form functional heteromeric and heterotypic channels. *Am J Physiol Cell Physiol*. 2007; 293(3):C1032–C1048.
11. Beltramello M, Piazza V, Bukauskas FF, Pozzan T, Mammano F. Impaired permeability to Ins(1,4,5) P3 in a mutant connexin underlies recessive hereditary deafness. *Nat Cell Biol*. 2005;7(1):63–69.
12. Bukauskas FF, et al. Clustering of connexin 43-enhanced green fluorescent protein gap junction channels and functional coupling in living cells. *Proc Natl Acad Sci U S A*. 2000;97(6):2556–2561.
13. Gaietta G, et al. Multicolor and electron microscopic imaging of connexin trafficking. *Science*. 2002;296(5567):503–507.
14. Sosinsky G. Mixing of connexins in gap junction membrane channels. *Proc Natl Acad Sci U S A*. 1995;92(20):9210–9214.
15. Inoshita A, et al. Postnatal development of the organ of Corti in dominant-negative Gjb2 transgenic mice. *Neuroscience*. 2008;156(4):1039–1047.
16. Kudo T, et al. Transgenic expression of a dominant-negative connexin26 causes degeneration of the organ of Corti and non-syndromic deafness. *Hum Mol Genet*. 2003;12(9):995–1004.
17. Minekawa A, et al. Cochlear outer hair cells in a dominant-negative connexin26 mutant mouse preserve non-linear capacitance in spite of impaired distortion product otoacoustic emission. *Neuroscience*. 2009;164(3):1312–1319.
18. Hasegawa S, et al. Apoptosis in neural crest cells by functional loss of APC tumor suppressor gene. *Proc Natl Acad Sci U S A*. 2002;99(1):297–302.
19. Schutz M, et al. The human deafness-associated connexin 30 T5M mutation causes mild hearing loss and reduces biochemical coupling among cochlear non-sensory cells in knock-in mice. *Hum Mol Genet*. 2010;19(24):4759–4773.
20. Tritsch NX, Yi E, Gale JE, Glowatzki E, Bergles DE. The origin of spontaneous activity in the developing auditory system. *Nature*. 2007;450(7166):50–55.
21. Lang H, et al. Contribution of bone marrow hematopoietic stem cells to adult mouse inner ear: mesenchymal cells and fibrocytes. *J Comp Neurol*. 2006;496(2):187–201.
22. Yum SW, Zhang J, Scherer SS. Dominant connexin26 mutants associated with human hearing loss have trans-dominant effects on connexin30. *Neurobiol Dis*. 2010;38(2):226–236.
23. Zhang J, Scherer SS, Yum SW. Dominant Cx26 mutants associated with hearing loss have dominant-negative effects on wild type Cx26. *Mol Cell Neurosci*. 2011;47(2):71–78.
24. Uyguner O, et al. The novel R75Q mutation in the GJB2 gene causes autosomal dominant hearing loss and palmoplantar keratoderma in a Turkish family. *Clin Genet*. 2002;62(4):306–309.
25. Kamiya K, Takahashi K, Kitamura K, Momoi T, Yoshikawa Y. Mitosis and apoptosis in postnatal auditory system of the C3H/He strain. *Brain Res*. 2001;901(1-2):296–302.
26. Anselmi F, et al. ATP release through connexin hemichannels and gap junction transfer of second messengers propagate Ca2+ signals across the inner ear. *Proc Natl Acad Sci U S A*. 2008;105(48):18770–18775.
27. Lin D, Zhou J, Zelenka PS, Takemoto DJ. Protein kinase Cgamma regulation of gap junction activity through caveolin-1-containing lipid rafts. *Invest Ophthalmol Vis Sci*. 2003;44(12):5259–5268.
28. Schubert AL, Schubert W, Spray DC, Lisanti MP. Connexin family members target to lipid raft domains and interact with caveolin-1. *Biochemistry*. 2002;41(18):5754–5764.
29. Zhang JT, Nicholson BJ. The topological structure of connexin 26 and its distribution compared to connexin 32 in hepatic gap junctions. *J Membr Biol*. 1994;139(1):15–29.
30. Ahmad S, et al. Restoration of connexin26 protein level in the cochlea completely rescues hearing in a mouse model of human connexin30-linked deafness. *Proc Natl Acad Sci U S A*. 2007;104(4):1337–1341.
31. Qu Y, et al. Early developmental expression of connexin26 in the cochlea contributes to its dominate functional role in the cochlear gap junctions. *Biochem Biophys Res Commun*. 2012;417(1):245–250.
32. White TW, Goodenough DA, Paul DL. Targeted ablation of connexin50 in mice results in microphthalmia and zonular pulverulent cataracts. *J Cell Biol*. 1998;143(3):815–825.
33. Gong X, et al. Disruption of alpha3 connexin gene leads to proteolysis and cataractogenesis in mice. *Cell*. 1997;91(6):833–843.
34. Zhang Y, Tang W, Ahmad S, Sipp JA, Chen P, Lin X. Gap junction-mediated intercellular biochemical coupling in cochlear supporting cells is required for normal cochlear functions. *Proc Natl Acad Sci U S A*. 2005;102(42):15201–15206.
35. Liang C, Zhu Y, Zong L, Lu GJ, Zhao HB. Cell degeneration is not a primary causer for Connexin26 (GJB2) deficiency associated hearing loss. *Neurosci Lett*. 2012;528(1):36–41.
36. Shibata H, et al. Rapid colorectal adenoma formation initiated by conditional targeting of the Apc gene. *Science*. 1997;278(5335):120–123.